WASHINGTON UNIVERSITY IN ST. LOUIS

The report from Washington University for the period follows.

ENGINEERING DEVELOPMENT OF SLURRY BUBBLE COLUMN REACTOR (SCBR) TECHNOLOGY

Nineteenth Quarterly Report for October 1 – December 31, 1999

(Budget Year 5 – 19th Quarter)

Chemical Reaction Engineering Laboratory (CREL)
Chemical Engineering Department
Washington University

Objectives for the Fifth Budget Year

The objectives set for the Fifth Budget Year (October 1, 1999 to September 30, 2000) are listed below.

- Extension of CARPT database to high superficial gas velocity in bubble column
- Extension CARPT/CT database to gas-liquid-solid system at high superficial gas velocity
- Evaluation of the effect of sparger design on the fluid dynamics of bubble columns using the CARPT technique
- Interpretation of LaPorte tracer data
- Further improvement in Computational Fluid Dynamics (CFD) using CFDLIB and Fluent

HIGHLIGHTS FOR THE 19TH QUARTER

During this quarter we focused on utilizing the collected Computer Automated Radioactive Particle Tracking (CARPT) data in developing numerical means for assessing the state of liquid flow and mixing in bubble columns. These related efforts were pursued in parallel: 1) evaluation of the global liquid re-circulation profiles via a one-dimensional global model; 2) dynamic simulation of fluid dynamics in a 14-cm diameter column and comparison of simulation results with available CARPT data; and 3) dynamic simulation of tracer distribution in the 14-cm diameter column. All of these efforts are continuing, but the accomplishments of the past quarter are summarized below.

1. One-dimensional model for liquid velocity distribution in a bubble column

- The database collected by Computer Automated Radioactive Particle Tracking (CARPT) and Computer Tomography (CT) is being systematically analyzed in search of patterns needed for scaleup.
- Scaling the data for liquid re-circulation velocity in a column of a single diameter with superficial gas velocity yields two velocity profiles. One is characteristic of bubbly flow, and the other of churn turbulent flow.
- Liquid re-circulation velocities increase with column diameter, and the proper scaling factor is being sought.
- Reynolds shear stress increases with superficial gas velocity and column diameter.

2. Dynamic simulation of 14-cm column and comparison with CARPT measurement

- The numerically predicted global gas holdup, based on CFDLIB codes, i.e., the dynamic heights of the column, is in good agreement with the experimental measurements.
- The mean liquid axial velocity profiles, calculated by time- and azimuthal-averaging of the numerically simulated velocity field, agree well with the CARPT measurement in the case of the churn turbulent regime.
- Comparison of the computed Reynolds stress distribution with CARPT data indicates that such comparison is far from straightforward and sheds additional insight into the use of turbulence models.

3. Dynamic simulation of tracer distribution in bubble columns

- The dynamic numerical simulation of passive scalars, in both liquid and gas phases, in a fully developed bubble column flow has been successfully accomplished using the three-dimensional CFDLIB code.
- The procedure for evaluating the averaged axial turbulent eddy diffusivity of the liquid phase is outlined.

- The preliminary results for the estimated axial liquid eddy diffusivity in a 14-cm diameter column operated at 2.4 cm/s superficial gas velocity is within the same range as the experimental data measured by CARPT.
- The effect of the gas distributor on turbulent eddy diffusivity is observed experimentally.

1. ONE-DIMENSIONAL MODEL FOR LIQUID VELOCITY DISTRIBUTION IN BUBBLE COLUMNS

1.1 Introduction

For design and scaleup purposes, it is important to have a reliable model to predict liquid recirculation. We used the CARPT/CT data base to develop a dimensionless model that should be useful for scaleup. The one-dimensional model equation for the time-averaged liquid velocity profile is

$$\frac{1}{r}\frac{d}{dr}\left[r\left(1-\bar{\varepsilon}\right)\left(\tau_t+\tau_m\right)\right]-\frac{dP}{dz}-\rho_l\left(1-\bar{\varepsilon}\right)g=0 \tag{1.1}$$

where the turbulence shear stress, τ_t, and the molecular viscous shear stress, τ_m, are respectively defined as

$$\tau_t=-\rho_l\left\langle u_r^{'}u_z^{'}\right\rangle \qquad\qquad \tau_m=\mu\frac{\partial\left\langle u_z\right\rangle}{\partial r}; \tag{1.2}$$

The azimuthal-averaged gas holdup, $\bar{\varepsilon}$, is a function of radial position. To validate a one-dimensional model, one needs information on the radial profile of the mean liquid velocity, $\left\langle u_z\right\rangle$, and Reynolds shear stress, $\left\langle u_r^{'}u_z^{'}\right\rangle$, which can be extracted from the CARPT database. In general, all these quantities are dependent on a number of process parameters such as superficial gas velocity, column size, physical properties of liquid and gas, and gas sparger type. Among these, the superficial gas velocity, U_g, and column diameter, D, are the two key parameters that dominate the fluid dynamics of a bubble column. In order to scale up and design bubble columns, a one-dimensional model in non-dimensional form is needed. Therefore, the column diameter and superficial gas velocity become the natural candidates for the characteristic integral length scale and velocity scale. To study the effects of D and U_g, we calculate and analyze $\left\langle u_z\right\rangle$ and $\left\langle u_r^{'}u_z^{'}\right\rangle$ for a 6 in. column operated at various superficial gas velocities and for 6, 8 and 18 in. columns operated at roughly the same superficial gas velocity of 12 cm/s.

1.2 Results and Discussion

Figure 1.1 shows the time-averaged liquid velocity profiles for the 14-cm diameter column at different operating conditions. As expected, $\left\langle u_z\right\rangle$ is proportional to the superficial gas velocity, U_g. The effect of U_g on the interstitial liquid velocities in the down-flow region is less than that in the up-flow region. This is due to the large area in the portion of the column where liquid flows downward and to the much higher liquid holdup in this region.

Scaling the liquid velocity by the superficial gas velocity, we reproduce the content of Figure 1.1 in Figure 1.2. It is immediately evident that the curves fall into two groups, one for U_g values of 2.4 and 4.8 cm/s, and the other for U_g values of 9.6 and 12 cm/s, which clearly represent the bubbly flow regime and churn turbulent flow regime, respectively. The fact that the non-dimensional profiles for the same flow regime overlap indicates that different similarity solutions may exist for different flow regimes. Notice that the non-dimensional liquid velocities of the turbulent flow group, i.e., U_g values of 9.6 and 12 cm/s, are smaller than those of the bubbly flow group, i.e., U_g values of 2.4 and 4.8 cm/s. This indicates that as flow transits from bubbly to churn turbulent, the dependence of liquid velocity on the superficial gas velocity, which is nearly linear in bubbly flow, changes.

Figure 1.3 shows the Reynolds shear stress, $\langle u_r' u_z' \rangle$. Again the difference between the bubbly and churn turbulent regime is clearly evident. Obviously the Reynolds shear stress is enhanced as the superficial gas velocity increases. However, at this time we are not sure about the proper scaling, which remains under investigation.

The effect of column size on liquid velocity is shown in Figure 1.4. It is not surprising that the non-dimensional liquid velocity profiles, $\langle u_z \rangle / U_g$, for 6 and 8 in. diameter columns are almost identical since the difference in column size is small. The results for the 18 in. column indicate that liquid velocity increases significantly as column size increases, which implies that the non-dimensional liquid velocity should be a function of a non-dimensional coefficient that contains both column diameter D and superficial gas velocity U_g. Finally, Figure 1.5 shows the effect of column size on the Reynolds shear stress. The trend is that $\langle u_r' u_z' \rangle$ increases as the column diameter becomes larger.

2. DYNAMIC SIMULATION OF 14-CM COLUMN AND COMPARISON WITH CARPT MEASUREMENT

2.1 Introduction

We have been working on the three-dimensional dynamic simulations of bubble columns for a period of time. One of the objectives is to perform the simulation for several superficial gas velocities for which we have CARPT data for liquid velocity. One important issue in gas-liquid Eulerian/Eulerian simulation is how to model the turbulence of the continuous phase (in this case, the liquid) properly. To study this issue, we present the results for two cases: one in the bubbly flow regime, the other in the churn turbulent regime.

In a turbulent flow, the the velocity field can be expressed as

$$u_i = \langle u_i \rangle + u_i' \tag{2.1}$$

The well-known, one-dimensional model equation for the time-averaged liquid velocity profile is

$$\frac{1}{r}\frac{d}{dr}\left[r\left(1-\bar{\varepsilon}\right)\left(\tau_t+\tau_m\right)\right]-\frac{dP}{dz}-\rho_l\left(1-\bar{\varepsilon}\right)g=0 \tag{2.2}$$

where the turbulence shear stress, τ_t, and the molecular viscous shear stress, τ_m, are respectively defined as

$$\tau_t=-\rho_l\left\langle u_r^{'}u_z^{'}\right\rangle \tag{2.3}$$

and

$$\tau_m=\mu\frac{\partial\left\langle u_z\right\rangle}{\partial r}; \tag{2.4}$$

From a CARPT measurement, one can directly evaluate the total Reynolds stress, i.e., Equation (2.3). Since the turbulence contains large scales, $u_i^{''}$, and small scales, $u_i^{'''}$, the velocity field, (1.1), can be further decomposed into

$$u_i=\left\langle u_i\right\rangle+u_i^{''}+u_i^{'''} \tag{2.5}$$

In a numerical simulation, it is very difficult to resolve the small turbulence scales, $u_i^{'''}$. However, the effect of this part can be accounted for by a properly chosen turbulence model. The velocity field generated from such simulation would then be given by

$$u_i=\left\langle u_i\right\rangle+u_i^{''} \tag{2.6}$$

where the average $\left\langle u_i\right\rangle$ now incorporates the small fluctuations. Therefore, the Reynolds shear stress evaluated from this velocity field is $-\rho_l\left\langle u_r^{''}u_z^{''}\right\rangle$. In terms of numerically predicted values, the total Reynolds stress, τ_t, can then be expressed as

$$\tau_t=\mu_t\frac{\partial\left\langle u_z\right\rangle}{\partial r}-\rho_l\left\langle u_r^{''}u_z^{''}\right\rangle+f \tag{2.7}$$

Here μ_t is the modeled eddy viscosity, which accounts for the effect of small-scale turbulence, and f represents the possible interaction between large and small scales due to the non-linear dependence of the Reynolds stress on the velocity fluctuations. (It should be noted that no information on f can be obtained from a simulation using turbulence models.) In our current simulations, a model for bubble-induced turbulence is used to evaluate μ_t:

$$\mu_t\propto\varepsilon w_s d_b \tag{2.8}$$

where ε , w_s and d_b denote the local gas holdup, the slip velocity between the bubble and liquid (again a local value) and the bubble diameter, respectively. It is apparent that this model is like a localized mixing length turbulence model. The turbulence scales of bubble size or smaller would be modeled by Equation (2.8), and any scale larger than this would be solved by simulation, the results of which would then give the second term of the right-hand side of Equation (2.7).

2.2 Results and Discussion

For the 14-cm diameter column, the two cases with superficial gas velocities of 2.4 and 9.6 cm/s, which fall into bubbly flow and churn turbulent flow regimes, respectively, were simulated.

Figures 2.1 and 2.2 show the instantaneous gas volume fraction contours of the 14-cm diameter column in a fully developed state. The typical three-dimensional spiral structures are clearly observed. The purpose of showing these plots is to ensure that, qualitatively, this approach is not unreasonable.

Figure 2.3 shows the variation of the column's dynamic height with time. For both cases, i.e., U_g=2.4 and 9.6 cm/s, the columns are pre-filled with gas for numerical stability. The simulations start from t=0. The column with U_g=2.4 cm/s quickly reaches the steady state, while the one with U_g=9.6 cm/s approaches a stable level after about 120 seconds. As a measure of the global gas holdup, the numerically simulated dynamic heights are compared with the experimentally measured ones. Reasonable agreement, as shown by Figure 2.3, is obtained for both cases.

Figure 2.4 shows the instantaneous liquid velocity component in the axial direction at a central point of the column. For both cases, the nature of turbulence, i.e., multi-scale (refer here to the time scales), is observed. Particularly for the 2.4 cm/s case, the large-scale motion, i.e., the slow motion, is discerned. Further analysis requires energy spectrum.

In Figure 2.5 the numerically calculated time-averaged liquid axial velocity profiles are compared with those measured by the CARPT technique. Better comparison is found for the U_g= 9.6 cm/s case than for the U_g=2.4 cm/s. It can be seen that the velocity inversion point for U_g=2.4 cm/s for the numerically computed profile is significantly different from the experimentally observed value. On the other hand, the comparison for the gas superficial velocity of 9.6 cm/s is good, except for the near-wall region. However., such discrepancy close to the walls could be due to the inaccuracy of CARPT measurement in the near-wall region. In fact, the studies of CARPT data have shown that the occurrence of the radioactive particle in the near-wall region is much lower than the average occurrence at all other positions of the column. When the particle visits the wall region, it is mainly carried by the strong downward flow of the liquid streams. Therefore, the averaged values are likely to over-estimate reality. As the superficial gas velocity increases, the situation becomes more severe, as evident by comparison of Figures 2.5(a) and (b). This suggests the use of LDA for better measurements in the near-wall region.

Finally, Figure 2.6 compares the profiles of Reynolds stresses. As discussed earlier, what is really compared here is the $\langle u_r'' u_z'' \rangle$ calculated from the dynamic, numerically simulated liquid velocity field, with the $\langle u_r' u_z' \rangle$ calculated from the CARPT measurement. The former contains only the contribution from the large-scale fluctuations, while the latter represents contributions from all the scales measured by CARPT. In fact, due to the limitation of the CARPT technique, the Reynolds stress calculated based on measurement does not contain the contribution from the smallest turbulent fluctuations, which cannot be captured by the currently used large (d_p=2.3mm), neutrally boyant radioactive tracking particle. However, if the turbulence model used manages to cover a wider range of small-scale fluctuations than those missed by CARPT, then one would expect $\langle u_r' u_z' \rangle$ observed by CARPT to still be larger than $\langle u_r'' u_z'' \rangle$ computed by the model. Therefore, the numerically calculated Reynolds stress profile should be lower than the one from CARPT measurement.

For the case of churn turbulent flow, i.e., U_g=9.6 cm/s, as shown in Figure 2.6(b), the comparison of computed and measured velocity cross correlation is consistent with the above discussion. If the portion that has already been modeled is added, as indicated by the first term on the right-hand side of Equation (2.7) to the $\langle u_r'' u_z'' \rangle$, the summation should be very close to measured $\langle u_r' u_z' \rangle$, provided that the large/small interaction term, f, is small.

However, for bubbly flow, U_g=2.4 cm/s, this is not the case, as shown by Figure 2.6(a). The numerically computed profile for the velocity cross correlation is higher than the experimental one. Actually the intensity of turbulence is very low for this case. In addition to the unsatisfactory comparison of the mean velocity, as shown in Figure 2.5(a), this indicates that the turbulence model, such as given by Equation (2.8), may not be needed for the cases within the bubbly flow regime. In other words, for bubbly flow, a simulation without any turbulence model should be able to resolve all the scales that can be detected by the CARPT regime. This assertion will be tested in future work.

The flow condition and parameters used in the simulation are summarized in Table 2.1.

Table 2.1. Flow Condition Computational Parameters

	Column diameter (cm)	Superficial gas velocity U_g (cm/s)	Static liquid height (cm)	Bubble diameter used in drag law (cm)
Case 1	14	2.4	120	0.5
Case 2	14	9.6	98	1.5

3. Dynamic Simulation of Tracer Dispersion in Bubble Columns

3.1 Introduction

One of the major objectives of our ongoing modeling and dynamic simulation of bubble column flow is to study the liquid/gas dispersion and mixing. The widely used one-dimensional axial dispersion model requires the effective axial dispersion coefficient for which no suitable accurate correlation has been found to date. On the other hand, the two-dimensional convection-diffusion model requires axial and radial eddy diffusivities and the liquid velocity profile. It was demonstrated that such a model, with the velocity profile and eddy diffusivity values provided from the CARPT studies, can predict well the independently measured liquid tracer exit age density function (Degaleesan *et al.*, 1996, 1997). This implies that such a model can accurately predict bubble column reactor performance for the first-order reaction schemes and is a model of choice for mildly nonlinear reactions. Moreover, the parameters of the model need to be supplied, which, if based on experimentation, is a very expensive and tedious proposition. Therefore, we attempt here to obtain the modeled parameters by three-dimensional numerical simulation of the flow field and tracer spreading. In the current report, we verify the capability of the dynamic tracer simulation to evaluate the averaged liquid turbulent diffusivity.

Before a tracer simulation is started, one needs to generate a fully developed turbulent liquid/gas velocity field inside the bubble column. The Eulerian/Eulerian two-fluid model is selected to dynamically simulate the bubble driven flow. Following Drew (1983), below are the governing equations for the motion of gas-liquid flow in bubble columns, consisting of the continuity equation for each phase,

$$-\frac{\partial \varepsilon}{\partial t} + \nabla \cdot \left[(1-\varepsilon)\mathbf{u}_l \right] = 0 \qquad (3.1)$$

$$\frac{\partial \varepsilon}{\partial t} + \nabla . \left(\varepsilon \mathbf{u}_g \right) = 0 \qquad (3.2)$$

as well as the momentum equations for each phase,

$$\rho_l(1-\varepsilon)\left(\frac{\partial \mathbf{u}_l}{\partial t}+\mathbf{u}_l\cdot\nabla\mathbf{u}_l\right)=\rho_l(1-\varepsilon)\mathbf{g}-(1-\varepsilon)\nabla p-(\mathbf{M}_d+\mathbf{M}_{vm})+\nabla.[(1-\varepsilon)\sigma_l]+\nabla\cdot\left[(1-\varepsilon)\sigma_l^b\right] \tag{3.3}$$

$$\rho_g\varepsilon\left(\frac{\partial \mathbf{u}_g}{\partial t}+\mathbf{u}_g\cdot\nabla\mathbf{u}_g\right)=\rho_g\varepsilon\mathbf{g}-\varepsilon\nabla p+(\mathbf{M}_d+\mathbf{M}_{vm}) \tag{3.4}$$

The subscript 'l' and 'g' indicate the properties for the liquid phase and the gas phase, respectively, and ε denotes the volume fraction of the gas phase, i.e., local gas holdup. The inter-phase momentum exchange term, $\mathbf{M}_d$, which is caused by drag force acting on bubbles, is given by

$$\mathbf{M}_d=\frac{6\varepsilon(1-\varepsilon)}{\pi d_b^3}\mathbf{F}_d \tag{3.5}$$

in which the drag force, $\mathbf{F}_d$, is expressed as

$$\mathbf{F}_d=\frac{1}{8}\rho_l\pi d_b^2 C_D\left|\mathbf{u}_l-\mathbf{u}_g\right|(\mathbf{u}_l-\mathbf{u}_g) \tag{3.6}$$

where d_b represents the bubble diameter. For the drag coefficient, C_D, we use the following expression (Drew 1983):

$$C_D=max\left[\frac{24}{Re}\left(1+0.15\,Re^{0.687}\right),\ f\frac{8}{3}\frac{Eo}{Eo+4}\right] \tag{3.7}$$

in which

$$f=\left\{\frac{1+17.67(1-\varepsilon)^{9/7}}{18.67(1-\varepsilon)^{3/2}}\right\}^2 \tag{3.8}$$

The Eotvos number, Eo, and bubble Reynolds number, Re, are defined as

$$Eo\equiv E\,g\rho_c d_p^2/\gamma \tag{3.9}$$

and

$$\mathrm{Re}\equiv d_b\left|\mathbf{u}_l-\mathbf{u}_g\right|/\upsilon_l \tag{3.10}$$

respectively. γ and υ_l denote the surface tension and dynamic viscosity of the liquid phase, respectively. Additional inter-phase momentum exchange, $\mathbf{M}_{vm}$, caused by the added-mass force, is given by

$$\mathbf{M}_{vm}=\frac{1}{2}(1-\varepsilon)\varepsilon C_{vm}\left(\frac{D\mathbf{u}_l}{Dt}-\frac{D\mathbf{u}_g}{Dt}\right) \tag{3.11}$$

where the added-mass coefficient, C_{vm}, is taken to be

$$C_{vm} = 1 + 3.32\varepsilon + O(\varepsilon^2) \tag{3.12}$$

In the momentum equation for the liquid phase, Equation (3.3), we adopted a model for the bubble-induced stress, as proposed by Sato *et al.* (1981)

$$\sigma_c^b = \rho_c \nu_b^t (\nabla \boldsymbol{u}_l + \nabla \boldsymbol{u}_l^T) \tag{3.13}$$

in which the bubble-induced additional viscosity is calculated by

$$\nu_b^t = k_b \varepsilon d_b \left| \boldsymbol{u}_l - \boldsymbol{u}_g \right| \tag{3.14}$$

The empirical constant k_b takes a value from 0.2 to 0.6; in this simulation, the value is 0.4.

The Equations (3.1) to (3.14) consist of a complete two-fluid model for describing the turbulent motion in gas/liquid systems. The three-dimensional dynamic simulations for the cylindrical bubble columns operated at various conditions can then be performed by using CFDLIB, in which the two-fluid model above is implemented. Such simulations generate fully developed flow fields, i.e., $\boldsymbol{u}_l(\boldsymbol{x},t)$, $\boldsymbol{u}_g(\boldsymbol{x},t)$ and $\varepsilon(\boldsymbol{x},t)$. The tracer simulations can then be started. If we use some type of passive scalar, for example C, as the local tracer concentration for the liquid phase, the convection-diffusion equation for C is given by

$$\frac{\partial (1-\varepsilon)C}{\partial t} + \nabla \cdot \left[(1-\varepsilon) C \boldsymbol{u_l} \right] = D_m^l \nabla^2 C \tag{3.15}$$

in which D_m^l is the molecular diffusivity. Similarly the governing equation for the gas tracer is written as

$$\frac{\partial \varepsilon S}{\partial t} + \nabla \cdot \left[\varepsilon C \boldsymbol{u_g} \right] = D_m^g \nabla^2 S \tag{3.16}$$

where S is chosen to denote the local gas phase tracer concentration. Equations (3.15) and (3.16), which are also numerically implemented in CFDLIB, are then solved, together with the fluid dynamic equations, (3.1) to (3.4), to generate the tracer concentration as a function of time and location in the column, $C(\boldsymbol{x},t)$ and $S(\boldsymbol{x},t)$, for the liquid and gas phase, respectively. Since in bubble columns the dispersion of passive scalars is dominantly controlled by turbulence, the molecular diffusivities, D_m^l and D_m^g, can be taken as negligible and thus are given zero value during the simulations. It should be emphasized that during the tracer simulation, the fluid dynamic equations are still being solved continuously. Since the tracers are passive scalars, their existence in the column, either in liquid phase or in gas phase, do not change the fluid dynamics at all.

Assuming axisymmetric flow field in a bubble column and neglecting the molecular diffusivity, Equation (3.15) can be converted into the following form in terms of cylindrical coordinates,

$$\frac{\partial(1-\varepsilon)C}{\partial t}+\frac{1}{r}\frac{\partial(1-\varepsilon)ru_r C}{\partial r}+\frac{\partial(1-\varepsilon)u_z C}{\partial z}=\frac{1}{r}\frac{\partial}{\partial r}\left[D_{rr}(1-\varepsilon)r\frac{\partial C}{\partial r}\right]+\frac{\partial}{\partial z}\left[D_{zz}(1-\varepsilon)\frac{\partial C}{\partial z}\right] \tag{3.17}$$

where the coefficients D_{zz} and D_{rr} represent the axial and radial turbulent eddy diffusivities, respectively. They are related to the turbulent transport by the following definitions:

$$\left\langle u_z^{'}C^{'}\right\rangle \equiv -D_{zz}\frac{\partial C}{\partial z} \tag{3.18}$$

$$\left\langle u_r^{'}C^{'}\right\rangle \equiv -D_{rr}\frac{\partial C}{\partial r} \tag{3.19}$$

where $\langle\ \rangle$ represents the ensemble averaging. Equation (3.17) represents the averaged balance equation for the non-volatile (passive) species, and is a transient, two-dimensional convection-diffusion equation. The phasic averaging that has been performed to arrive at this equation (see Degaleesan 1997) refers to any time interval, which may be small or large.

Performing a volume integration of the above equation over a section of the column, as illustrated in Figure 3.1, one gets

$$\iint\frac{\partial\varepsilon C}{\partial t}dsdz+\iint\frac{\partial}{\partial z}(\varepsilon u_z C)dsdz=\iint\frac{\partial}{\partial z}\left(D_{zz}\varepsilon\frac{\partial C}{\partial z}\right)dsdz \tag{3.20}$$

in which $\int ds$ represents the area integration over the column's cross-section. The term involving the radial turbulent eddy diffusivity, D_{rr}, vanishes since the boundary condition of zero flux in radial direction at $r=R$ was imposed. The axial turbulent eddy diffusivity, D_{zz}, may be a function of r. However, the volume-averaged axial turbulent eddy diffusivity can be defined as

$$\overline{D}_{zz}=\frac{\iint\frac{\partial\varepsilon C}{\partial t}dsdz+\iint\frac{\partial}{\partial z}(\varepsilon u_z C)dsdz}{\iint\frac{\partial}{\partial z}\left(\varepsilon\frac{\partial C}{\partial z}\right)dsdz} \tag{3.21}$$

If the integration along the axial direction, z, extends from z_1 to z_2, as indicated in Figure 1, Equation (3.21) can be further written as

$$\overline{D}_{zz} = \frac{\iint \frac{\partial \varepsilon C}{\partial t} dsdz + \int \left[(\varepsilon u_z C)_{z2} - (\varepsilon u_z C)_{z1} \right] ds}{\int \left[\left(\varepsilon \frac{\partial C}{\partial z} \right)_{z2} - \left(\varepsilon \frac{\partial C}{\partial z} \right)_{z1} \right] ds} \tag{3.22}$$

To calculate the right-hand side of Equation (3.22), the liquid velocity field, $\boldsymbol{u}_l(\boldsymbol{x}, t)$, the gas holdup distribution, $\varepsilon(\boldsymbol{x}, t)$, and the tracer concentration distribution, $C(\boldsymbol{x}, t)$ are needed. In fact, all of these quantities are obtained from a dynamic tracer simulation, in which Equations (3.1) to (3.4) and (3.15) are numerically solved. In such a way, the volume-averaged turbulent eddy diffusivity of the liquid phase in a cylindrical bubble column can be evaluated numerically. Notice that $\overline{D}_{zz}$ in Equation (3.22) is still a function of time. In fact $\overline{D}_{zz}$ is calculated from the liquid velocity, local gas holdup and local tracer concentration at time t, as one can see from Equation (3.22). As with an ensemble averaging, $\overline{D}_{zz}$, which is now a volume-averaged quantity, should be further averaged over time to obtained the averaged turbulent eddy diffusivity. In the dynamic simulations presented here, the CFDLIB code outputs the time-dependent results every Δt second. Usually the tracer simulations for a 14-cm diameter column operated at 2.4 cm/s superficial gas velocity last about 20 to 30 seconds. For this particular case, the results show that the liquid tracer concentration reaches a nearly uniform distribution at about 15 seconds after the tracer-injection. The time interval for output, Δt, is set to 0.1 second. The averaged turbulent eddy diffusivity, $\langle D_{zz} \rangle$, is therefore calculated as,

$$\langle D_{zz} \rangle = \frac{1}{N} \sum_{n=1}^{N} \overline{D}_{zz}(t_0 + n\Delta t) \tag{3.23}$$

where t_0 denotes the time when the tracer is injected into the column and $N\Delta t$ represents the total time of the tracer simulation. Both Δt and N are adjustable according to the flow conditions and column geometry.

In this report, we present a preliminary result on the tracer simulation and the calculation of axial turbulent eddy diffusivity, as outlined above, for the liquid phase in a three-dimensional bubble column. The bubble column being simulated is 14 cm in diameter and operated at a gas superficial velocity of 2.4 cm/s.

3.2 Results and Discussion

To ensure an accurate evaluation of the dispersion coefficient, the numerical tracer simulation can only be started when the flow field of the column reaches a statistically quasi-steady state. Since the tracer dispersion in the axial direction is largely controlled by the mean axial momentum and its fluctuation, we calculated the time- and azimuthal-averaged profiles of the liquid axial velocity, $\langle u_z \rangle$, and the axial turbulence intensity, $\langle u_z^{'} u_z^{'} \rangle$. For the 14-cm diameter column operated at U_g=2.4 cm/s, two experiments were conducted. One was for the column with perforated plate type **6A** as the gas distributor, and the other was for the column with distributor **6B**. Figure 3.2 depicts the gas distributors. In Figure 3.3, comparisons are made between the computed numerical values and the corresponding experimental data. As this figure shows, using different gas distributors does not induce large differences in the mean axial velocity, and the computed profile is satisfactorily close to the experimental ones. However, the effect of gas distributors on turbulence intensities is significant. As shown in Figure 3.3, the axial liquid turbulence intensity for the column with the **6B** distributor is about three times larger than that for the column with distributor **6A**. The numerical profile lies in between. Notice that in a numerical simulation, the type of gas distributor was not exactly matched due to the limited mesh resolution. As shown in Figure 3.2, the gas is introduced through the numerical cells in the shaded area only. With the current mesh system, this matches most closely the real gas distributors **6A** and **6B**.

Figure 3.4 shows the time evolution of liquid tracer concentration in the 14-cm diameter column operated at a superficial gas velocity of 2.4 cm/s. An impulse of tracer is injected at the center of the column (r=0) and close to the bottom (z=3 cm). The injection is made when the flow field reaches the fully developed state. Due to liquid recirculation, i.e., batch flow, the liquid tracer cannot escape the column. Therefore, the tracer concentration eventually approaches a uniform pattern. On the other hand, as shown in Figure 3.5, the gas tracer eventually exits the column. One can also observe the downward dispersion of the gas tracer due to the carrying of gas bubbles by liquid back flow near the wall region.

Figure 3.6 displays the liquid tracer concentrations observed at different axial locations as functions of time. C_0 is proportional to the cross-sectional average concentration and is defined as

$$C_0(z) \equiv \int C ds \tag{3.24}$$

where the area integral, $\int (\ ) ds$, is taken over the cross section at a axial location, z. It can be seen that at the time of 10 seconds after the tracer injection, there is still a spatial non-uniformity of tracer distribution. The complete simulation indicates that after about 15 seconds the tracer concentration field reaches uniform distribution along the z direction. From this simulation the liquid velocity, liquid holdup, tracer concentration and the spatial gradient of the tracer concentration are sampled every 0.1 second. The averaged axial turbulent eddy diffusivity is calculated by using Equations (3.22) and (3.23). This result is listed in Table 3.1, in which the experimentally measured values of eddy diffusivity obtained by CARPT for distributors **6A** and **6B** are also listed. The effect of the gas distributor on diffusivity is quite significant. However, the calculated turbulent eddy diffusivity is within the same range as the experimental data. It should be pointed out that the calculated turbulent diffusivity should be independent of the location of tracer injection. A reliable value can only be obtained by performing a series of tracer simulations with different locations of the initial injection.

Table 3.1 Flow Condition Computational Parameters

D (cm)	U_g (cm/s)	H_s (cm)	d_b (cm)	Computed $\langle D_{zz} \rangle$ (cm^2/sec)	$\langle D_{zz} \rangle$ **6A** (cm^2/sec)	$\langle D_{zz} \rangle$ **6B** (cm^2/sec)
14	2.4	120	0.5	72	48	75

Reference

Degaleesan, S., S. Roy, S.B. Kumar, and M.P. Dudukovic, ``Liquid mixing based on convection and turbulent dispersion in bubble columns," *Chem. Eng. Sci*. 51, 1976 (1996).

Degaleesan, S., "Fluid dynamic measurements and modeling of liquid mixing in bubble columns," D. Sci. Thesis, Washington University in St. Louis, (1997).

Degaleesan, S., M.P. Dudukovic, B.A. Toseland, and B.L. Bhatt, ``A two compartment convective-diffusive model for slurry bubble column reactor," *Ind & Eng. Chem. Res*., 36 (11), 4670 (1997).

Drew, D.A. "Mathematical modeling of two-phase flow," *Ann. Rev. Fluid Mech*., 15, 261 (1983).

Sato, Y., M. Sadatomi and K. Sekoguchi, "Momentum and heat transfer in two-phase bubble flow I," *Int. J. Multiphase Flow*, 7, 167 (1981).

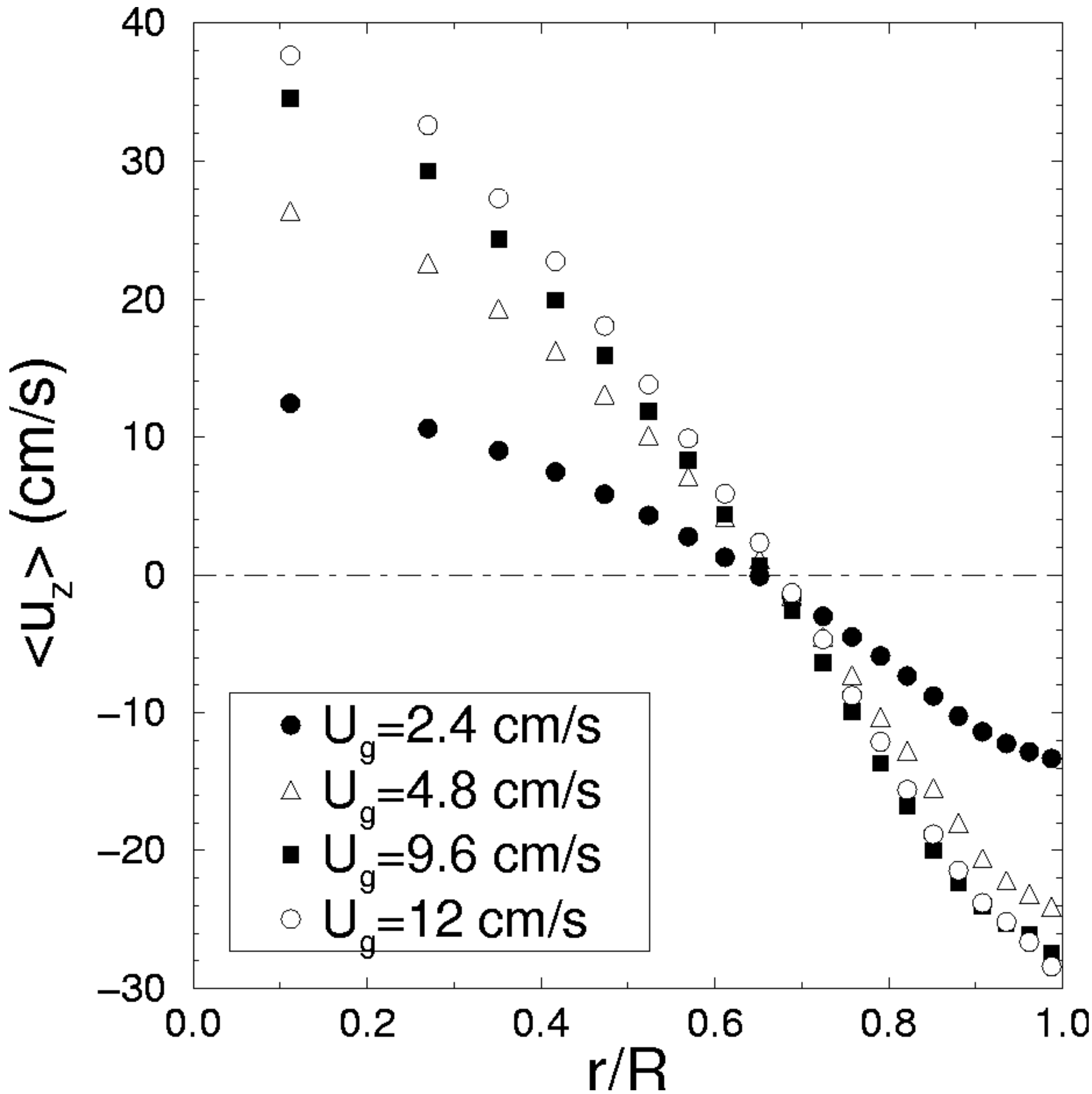

Figure 1.1 Mean Axial Liquid Velocity of 14-cm (D=6 in.) Column Operated at Different Superficial Gas Velocities, U_g.

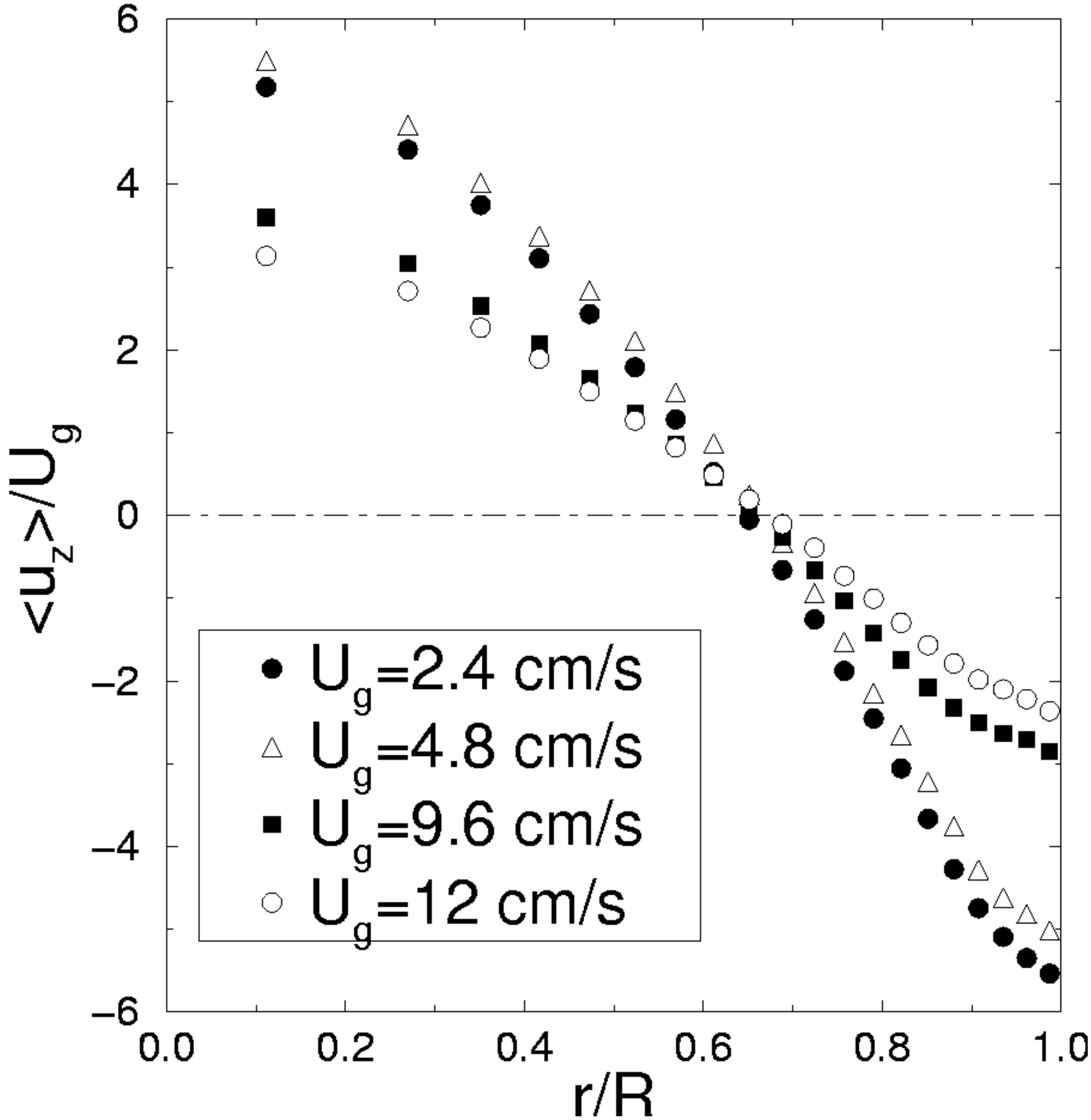

Figure 1.2 Non-Dimensional Mean Axial Liquid Velocity for 14-cm (D=6 in.) Column Operated at Different Superficial Gas Velocities, U_g. (The velocities are scaled by their superficial gas velocities.).

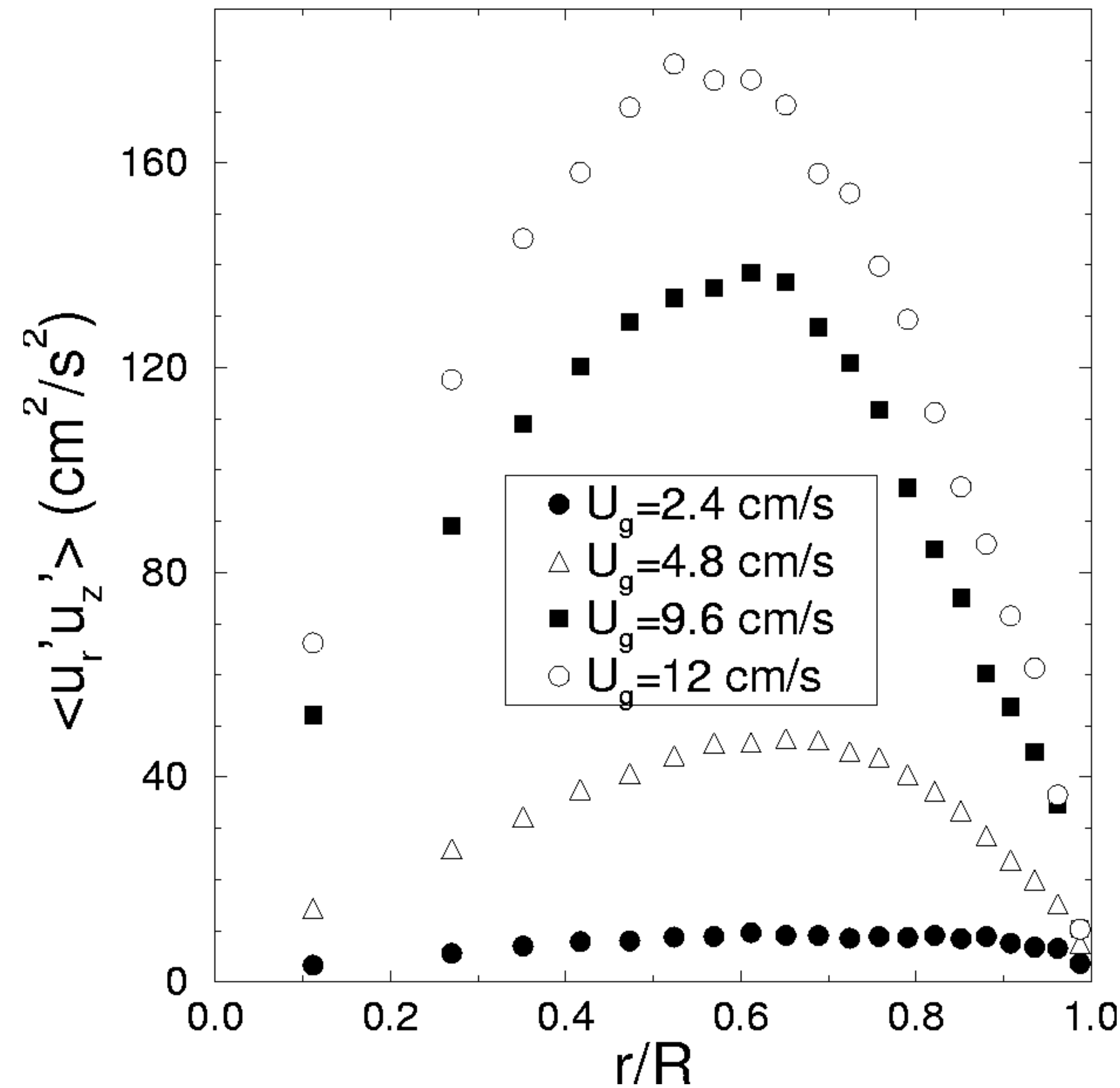

Figure 1.3 The Radial Distributions of Reynolds Shear Stress, $\langle u_r' u_z' \rangle$, in 14-cm (D=6 in.) Column Operated at Different Superficial Gas Velocities, U_g

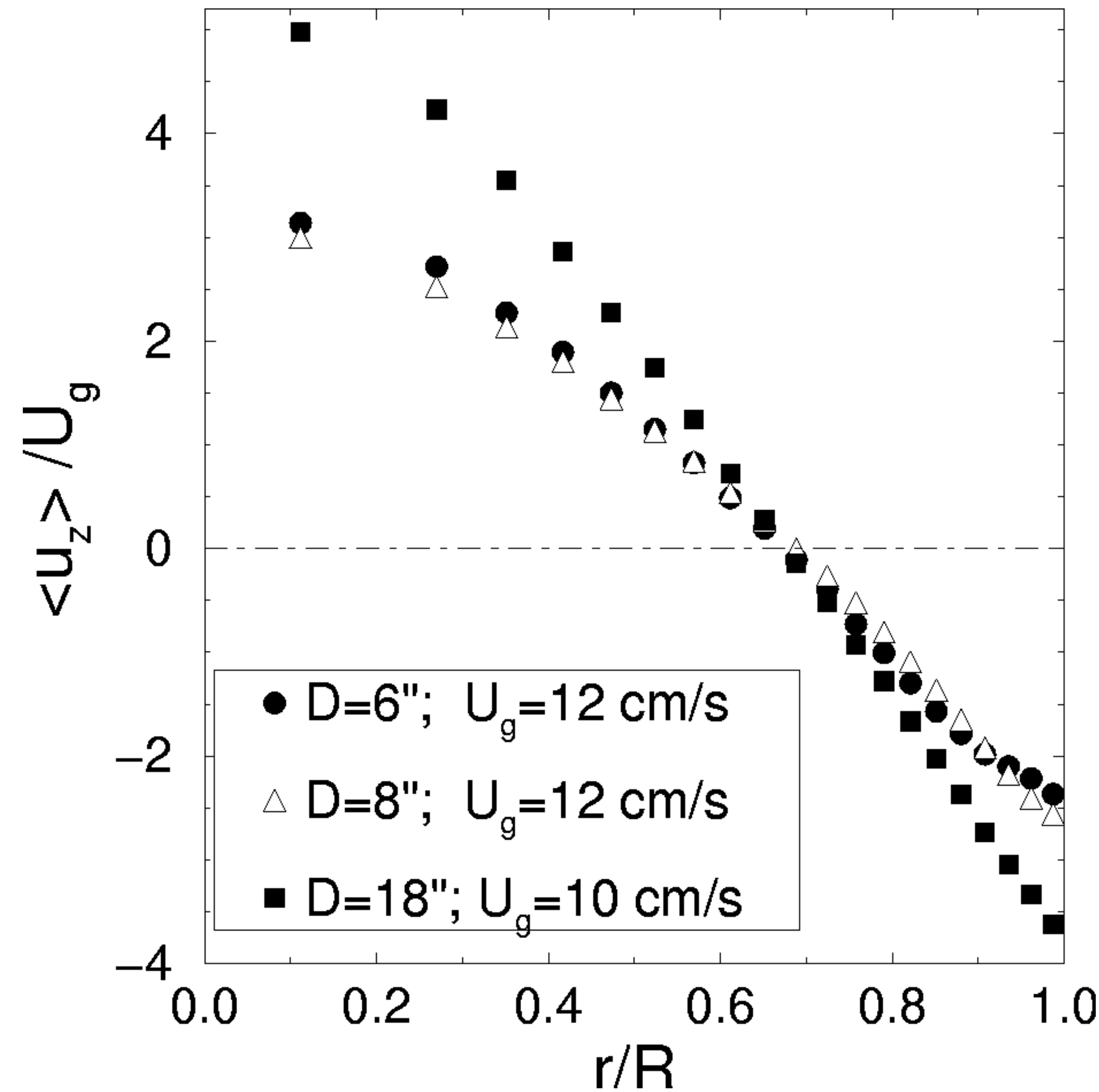

Figure 1.4 Non-Dimensional Mean Axial Liquid Velocity for Different-Sized Columns Operated at Approximately the Same Superficial Gas Velocities, U_g

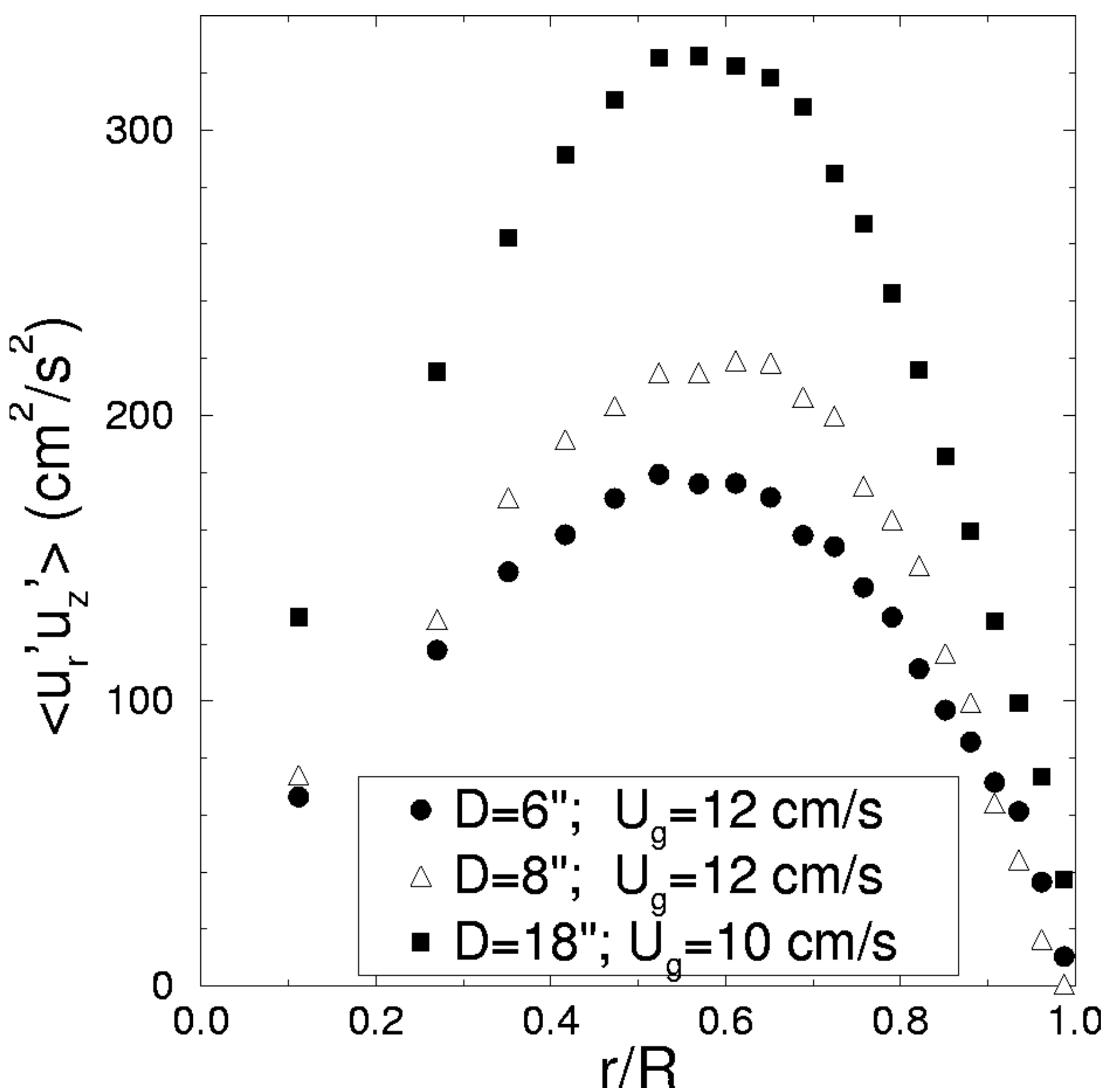

Figure 1.5 The Radial Distributions of Reynolds Shear Stress, $\langle u_r' u_z' \rangle$, in Different-Sized Columns Operated at Approximately the Same Superficial Gas Velocity, U_g

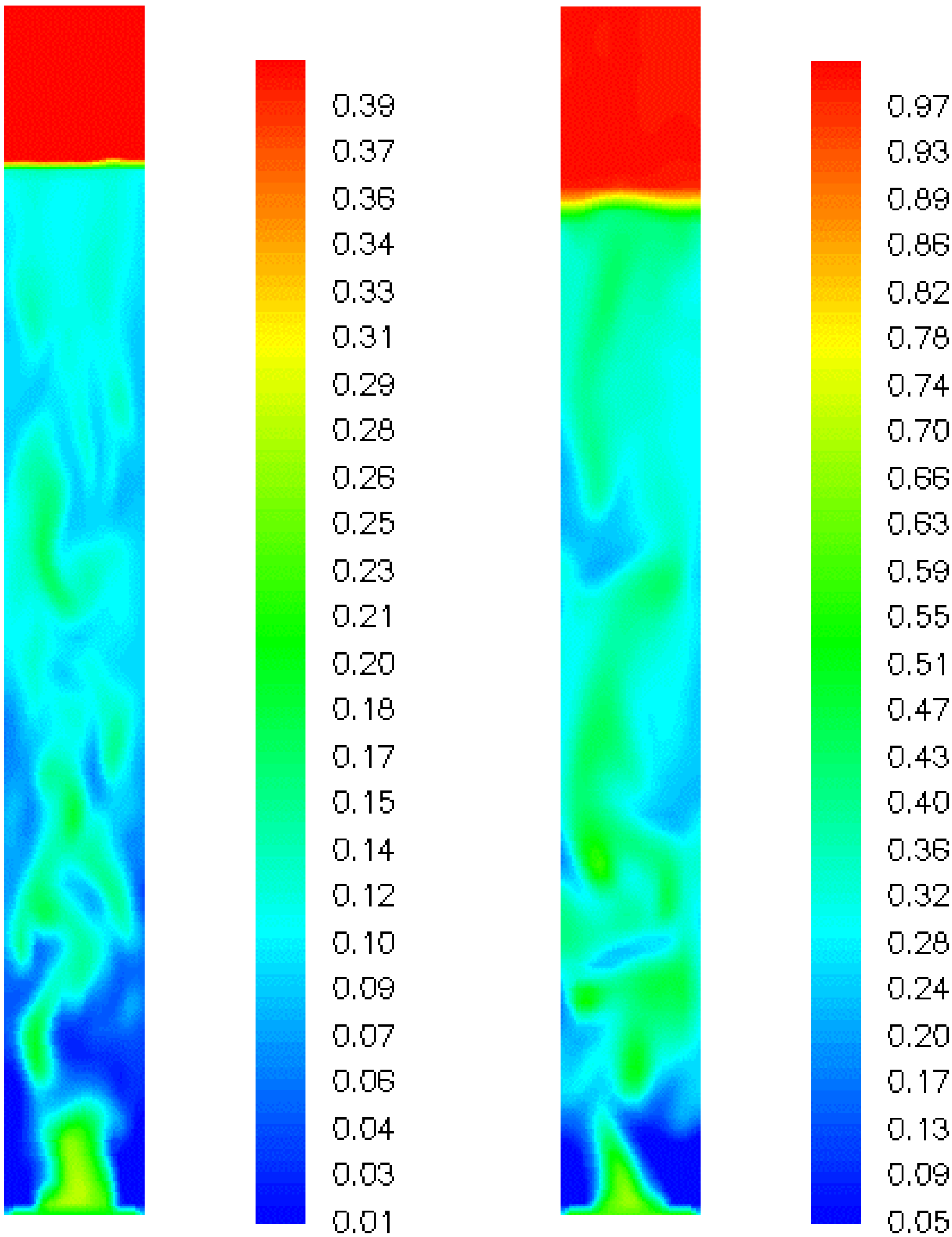

(1) U_g=2.4 cm/s. **(2)** U_g=9.6 cm/s.

Figure 2.1 Instantaneous Gas Holdup Contours on a Plane Cutting Through the Center of the Column. Column Diameter, D=14 cm.

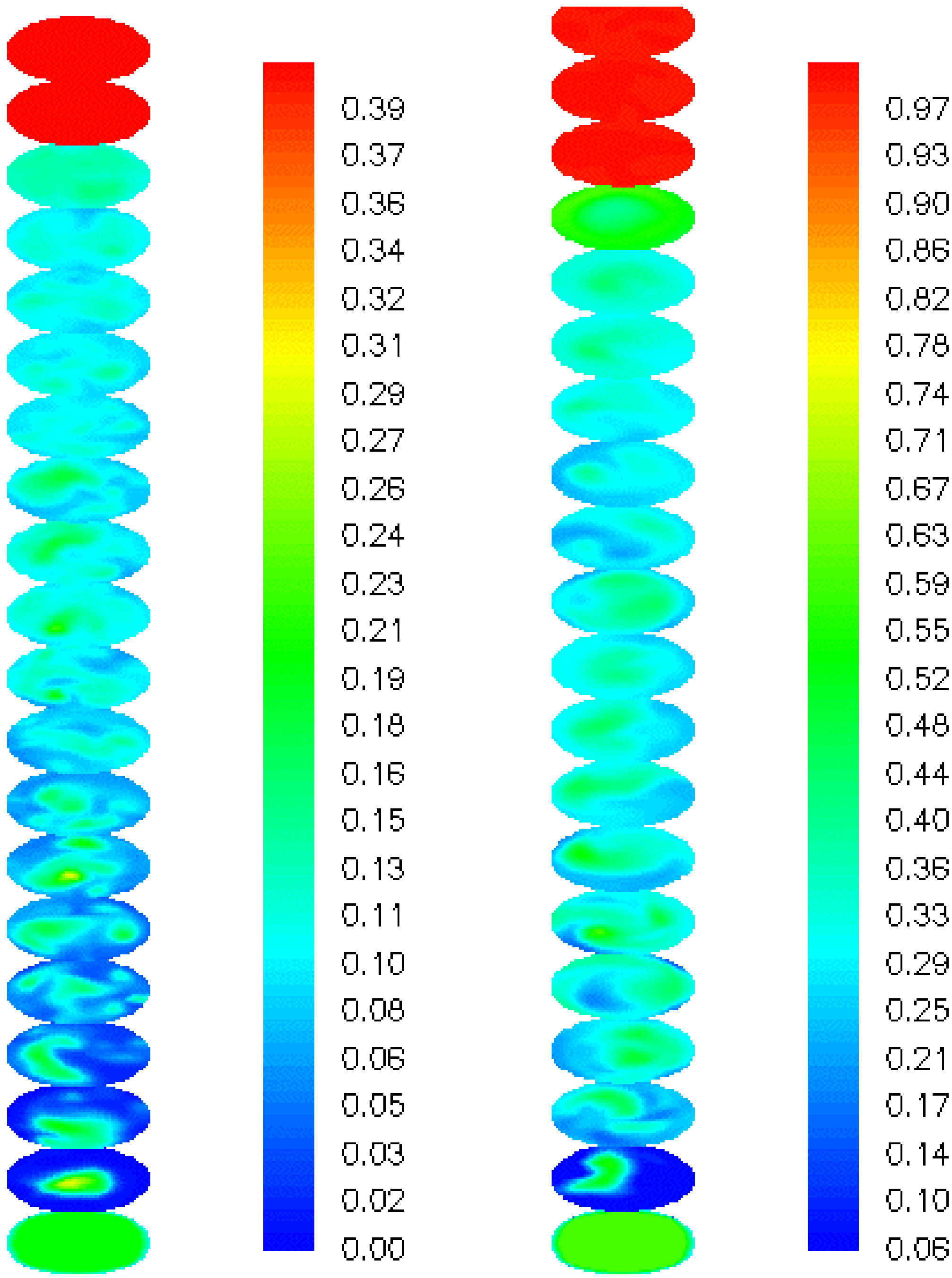

(1) U_g=2.4 cm/sec. (2) U_g=9.6 cm/sec.

Figure 2.2 Instantaneous Gas Holdup Contours on Cross-Sectional Planes (3D view) Column. (Column diameter (D)=14 cm)

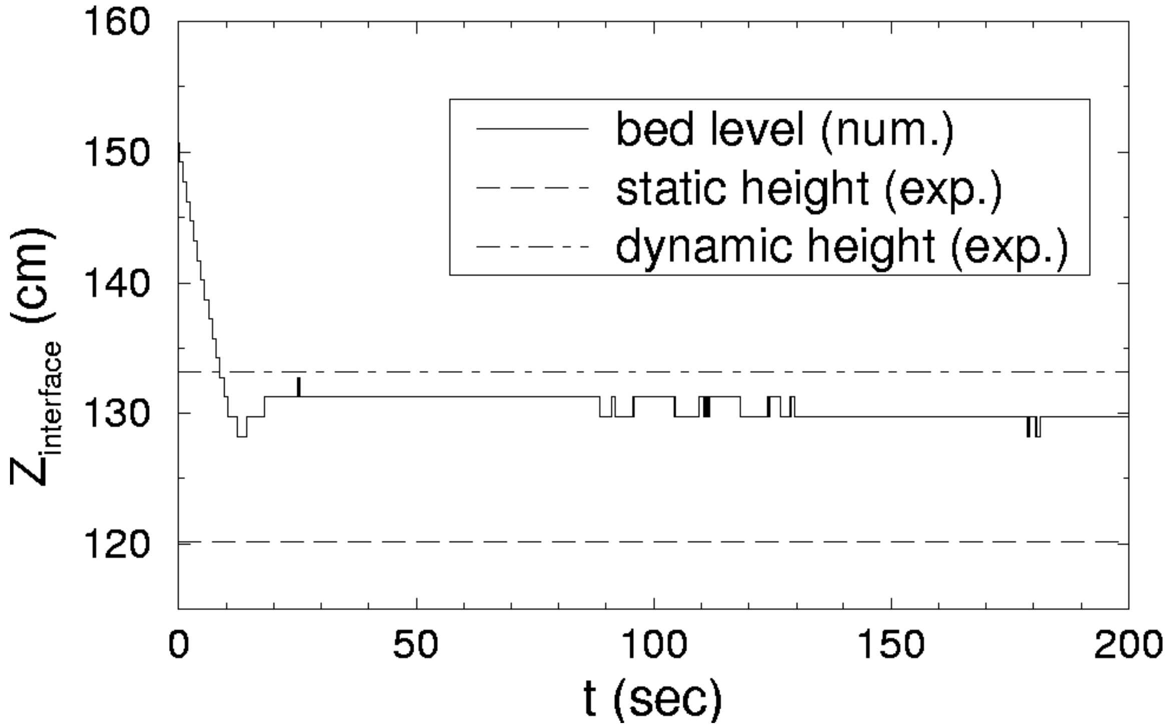

(a) U_g=2.4 cm/s

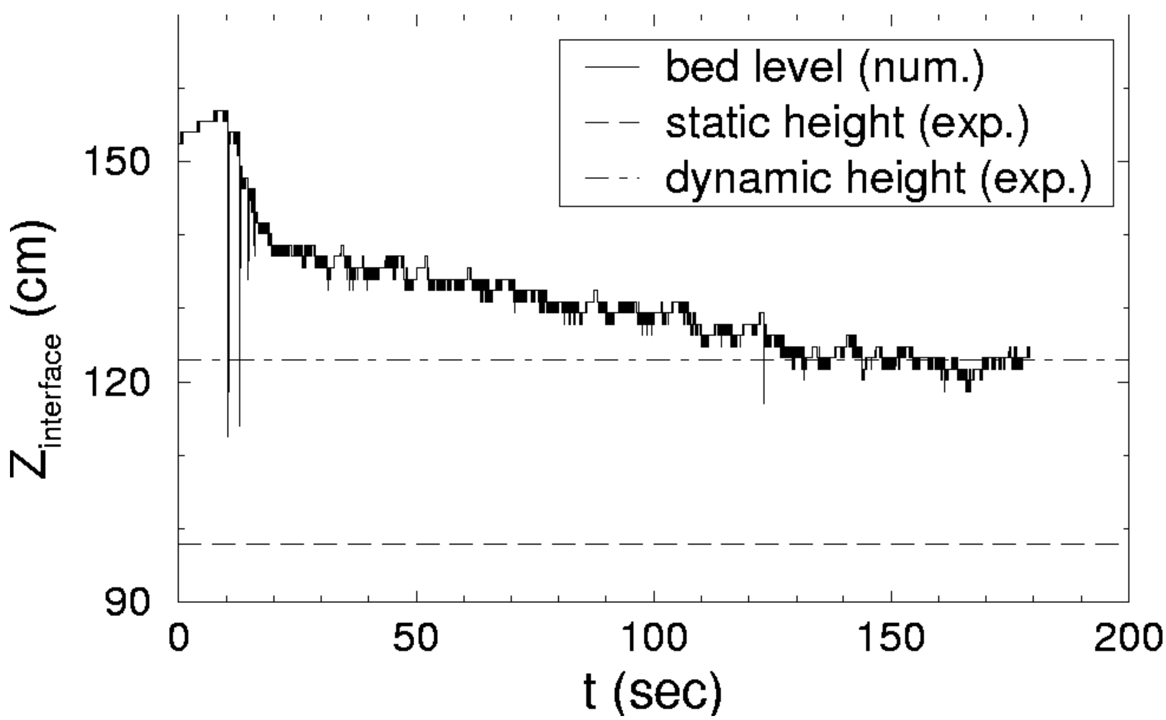

(b) U_g=9.6 cm/s

Figure 2.3 Variation of Column's Dynamic Height with Time. (Column diameter (D)=14 cm)

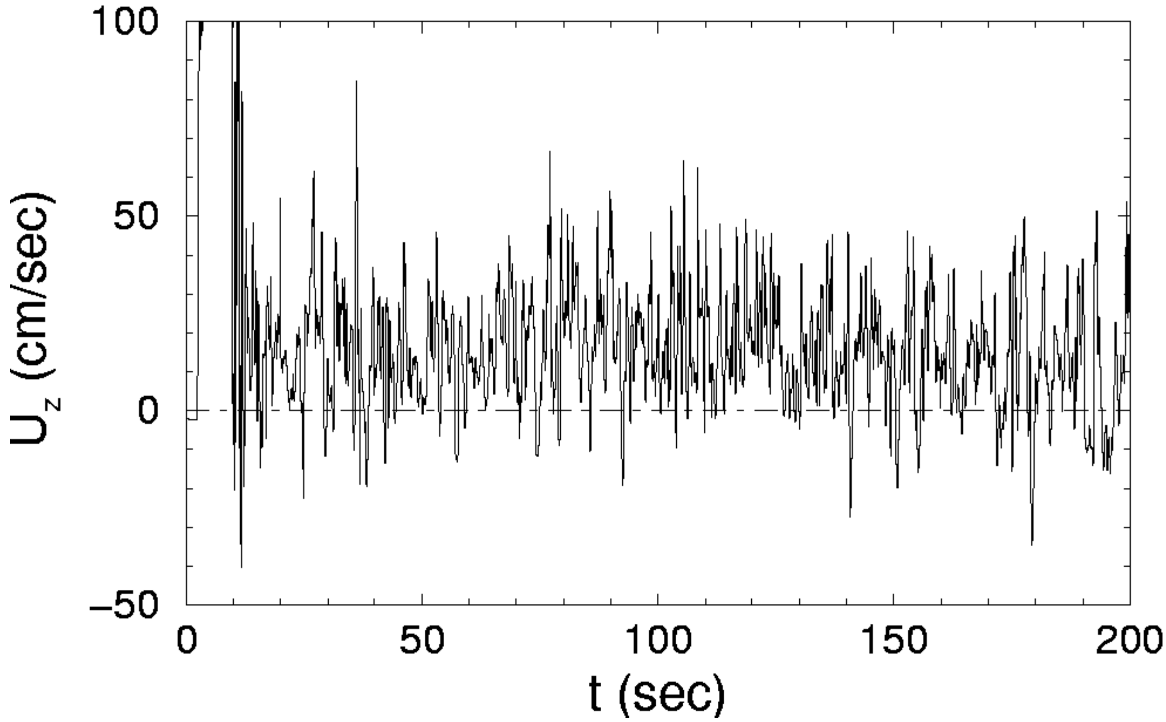

(a) U_g=2.4 cm/s

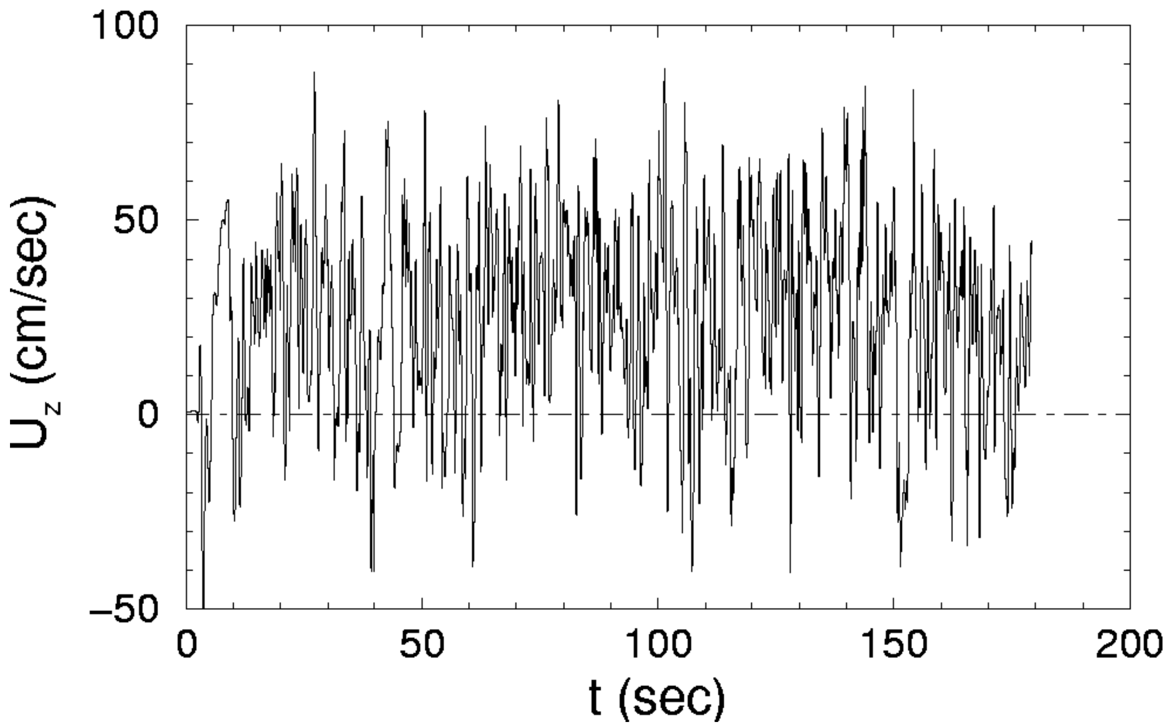

(b) U_g=9.6 cm/s

Figure 2.4 The Instantaneous Liquid Axial Velocity at the Center Point of the Column. (Column diameter (D)=14 cm)

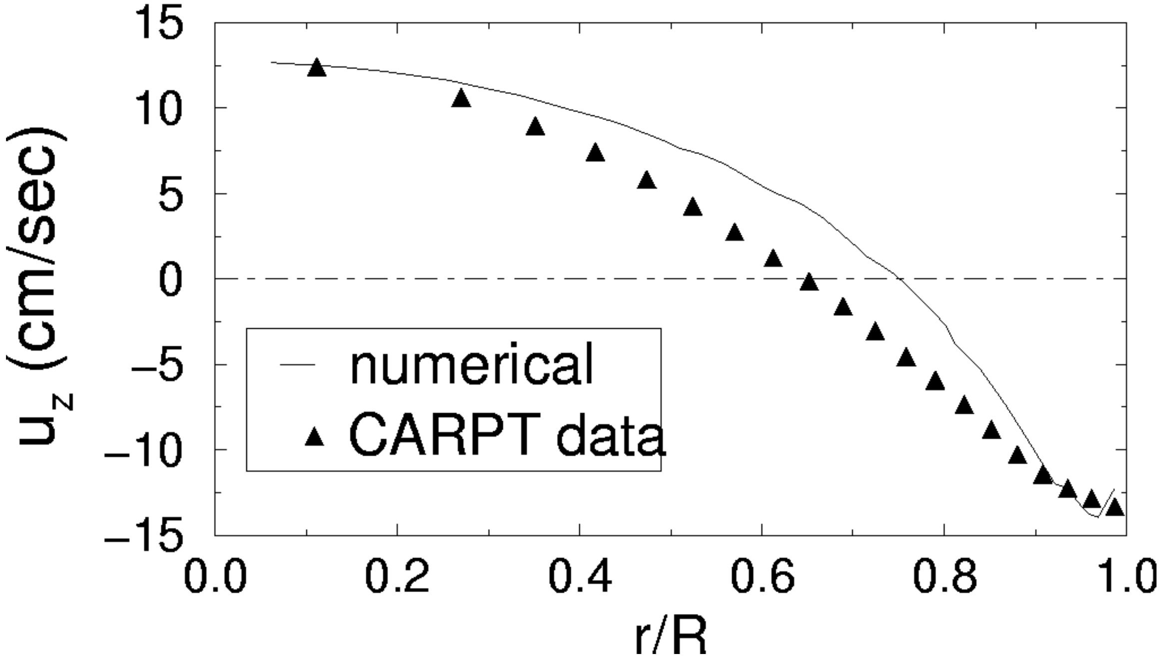

(a) U_g=2.4 cm/s

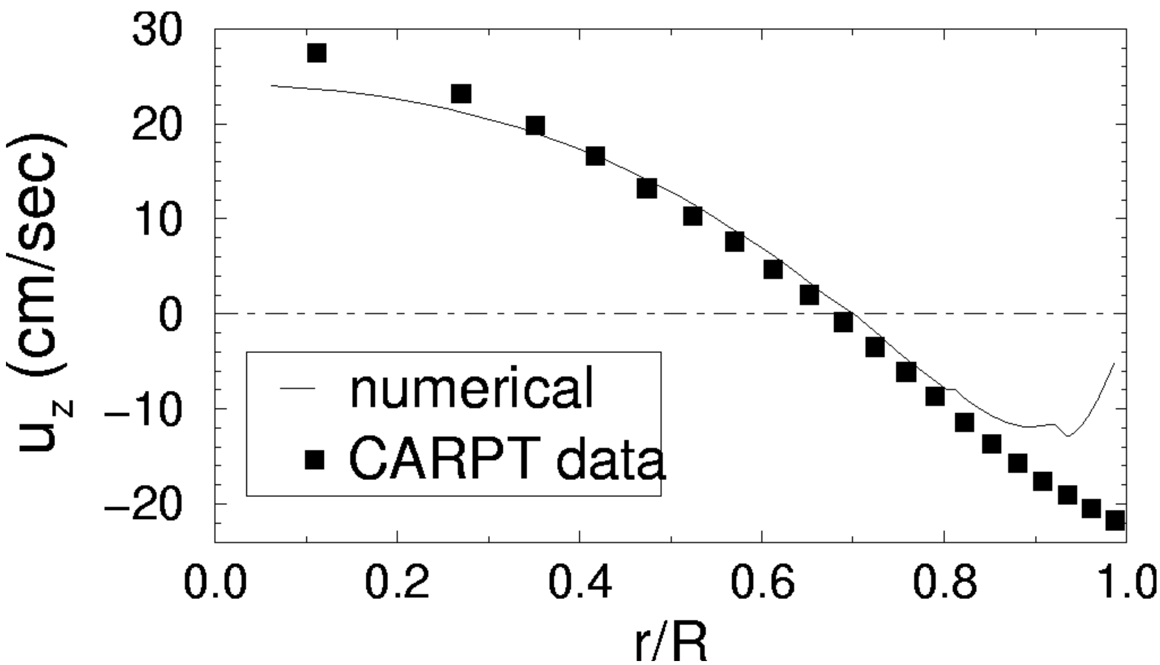

(b) U_g=9.6 cm/s

Figure 2.5 Time-Averaged Liquid Axial Velocity Profiles - Numerical and Experimental. (D=14 cm)

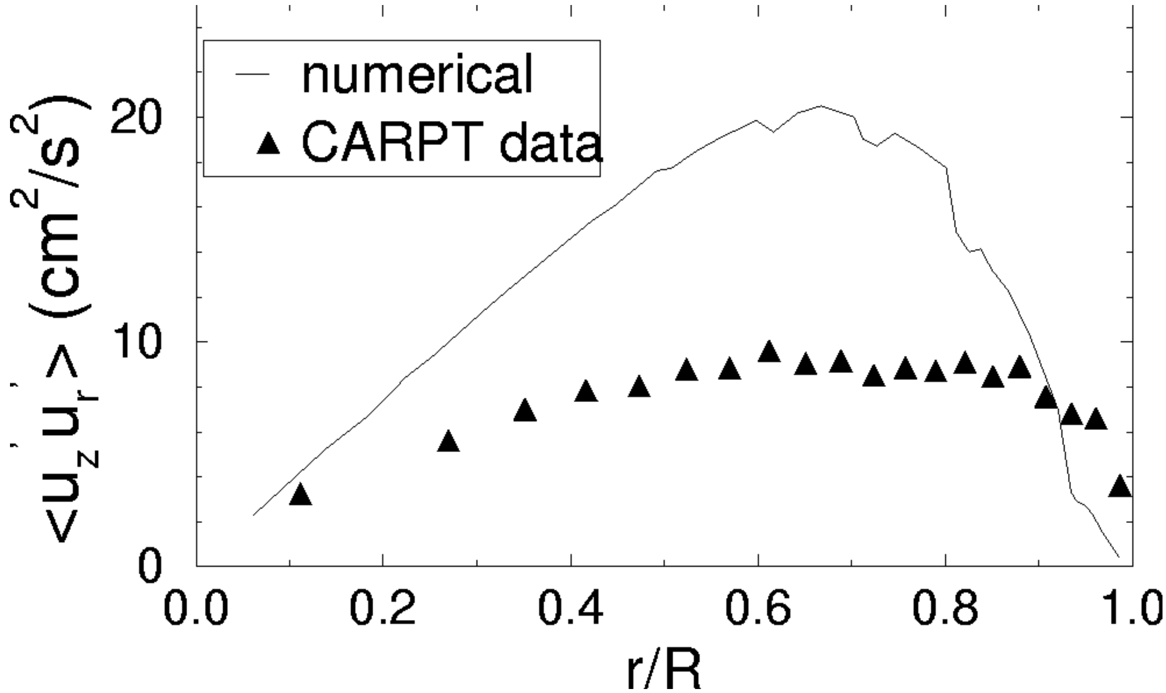

(a) U_g=2.4 cm/s

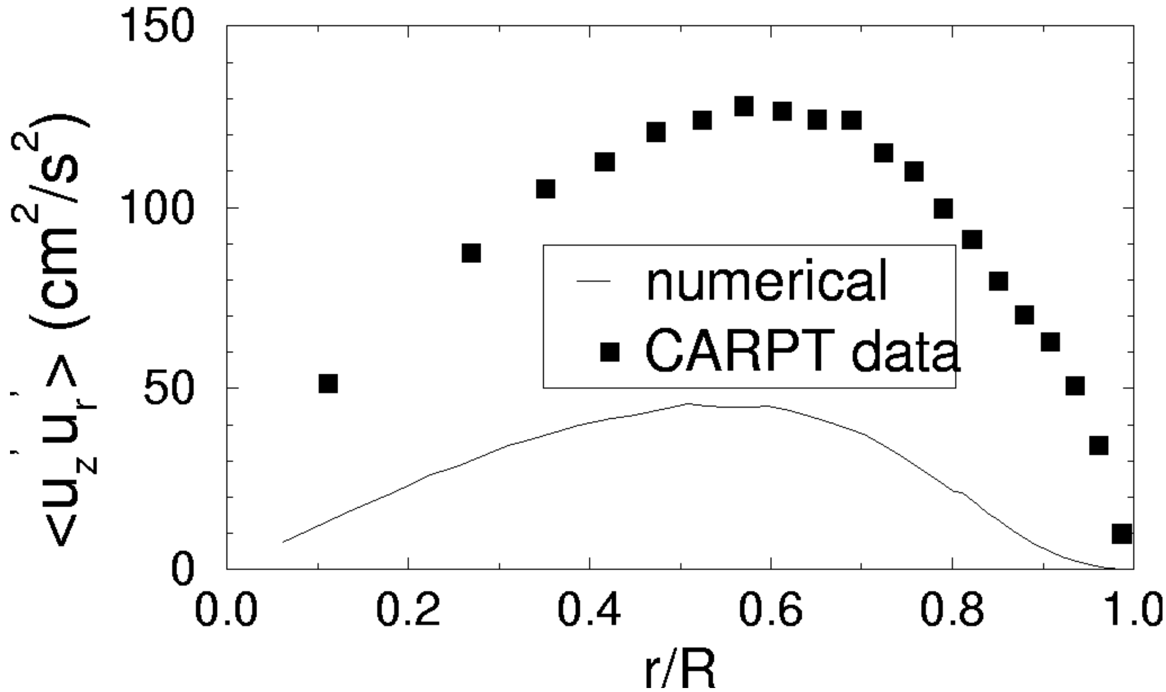

(b) U_g=9.6 cm/s

Figure 2.6 Reynolds Stress, $\langle u_r' u_z' \rangle$, Profiles - Numerical and Experimental. (D=14 cm)

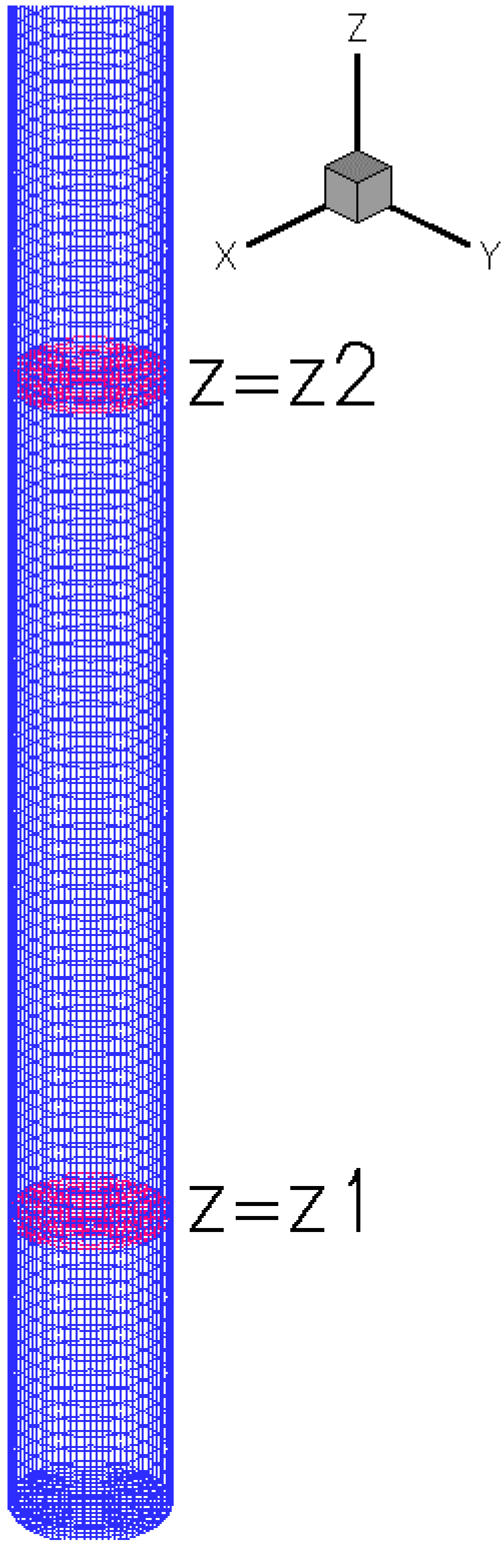

Figure 3.1 Computational Mesh System for Fluid Dynamic and Tracer Simulation in Bubble Columns

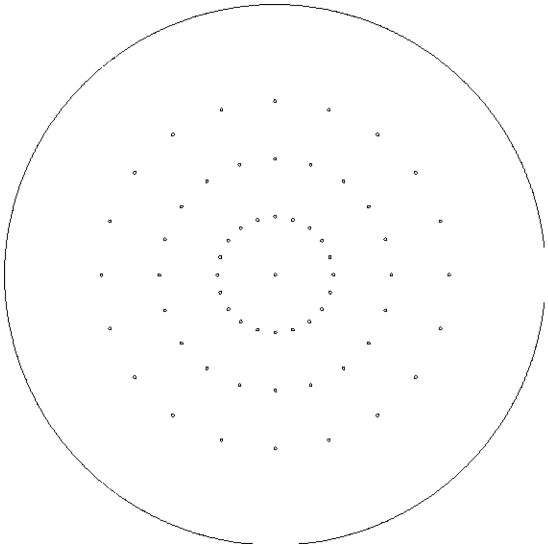

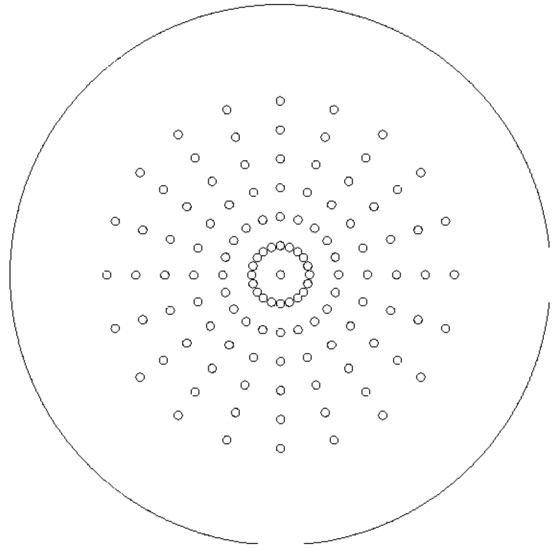

6A **6B**

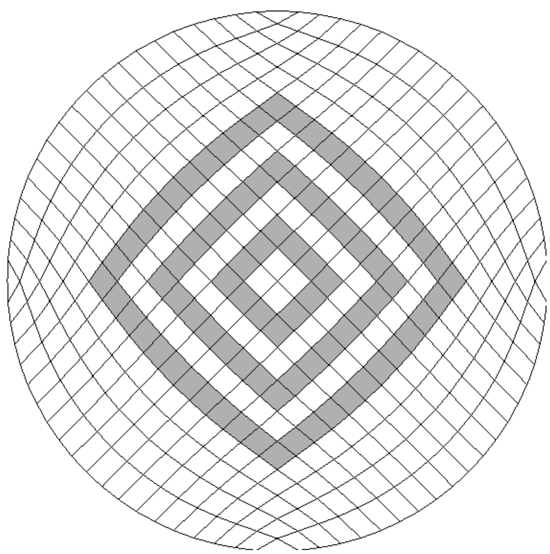

Computational mesh

Figure 3.2 The Perforated Plate Gas Distributors used on the 14-cm Diameter Column: 6A (holes of 0.4 mm; 3 concentric circles; 0.05% porosity) and 6B (holes of 1 mm; 6 concentric circles; 0.62% porosity). (Computational mesh at column's bottom: the gas is injected through the shadowed area only.)

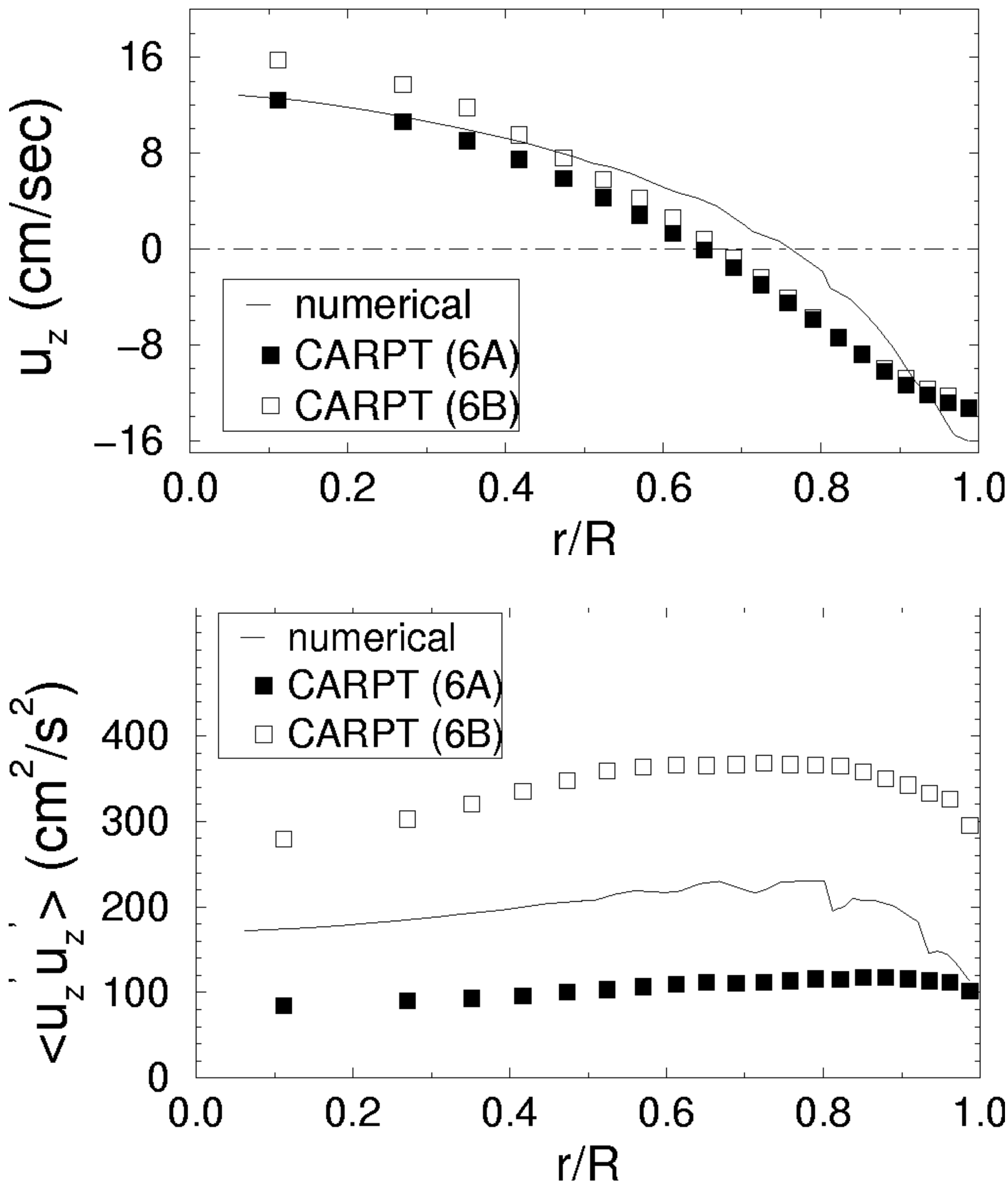

Figure 3.3 Time-Averaged Liquid Axial Velocity, $\langle u_z \rangle$, and Turbulence Intensity, $\langle u_z' u_z' \rangle$, for 14-cm Column Operated at Superficial Gas Velocity of U_g=2.4 cm/s. (The experimental data, from CARPT measurement, are for two different perforated plate gas distributors: 6A and 6B.)

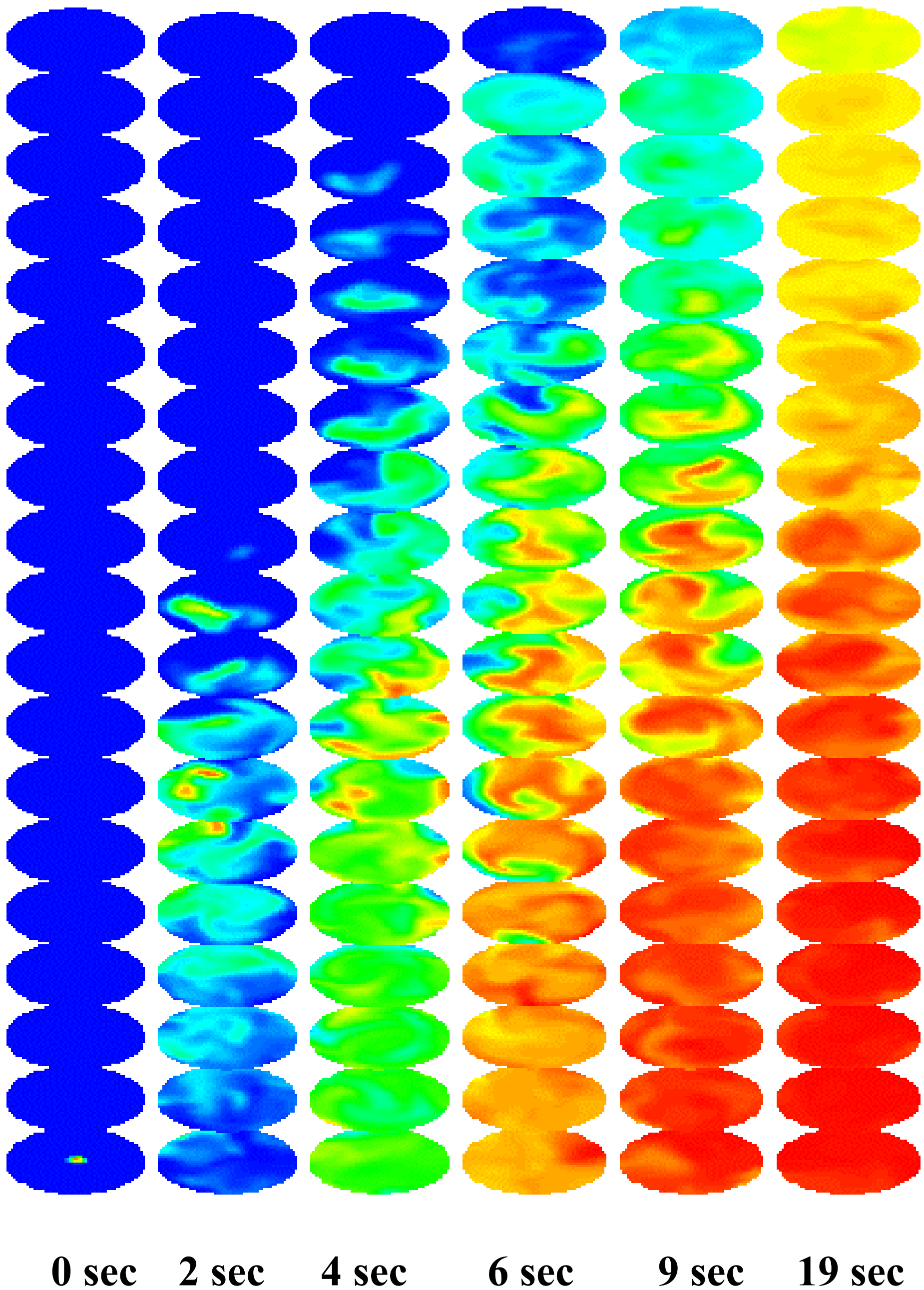

Figure 3.4 Time Evolution of the Liquid Tracer Concentration Inside a 14-cm Diameter Column at U_g=2.4 cm/s. [The tracer is released at the center of the column, near the bottom, at time t=0. There is no net flow of liquid (batch liquid).]

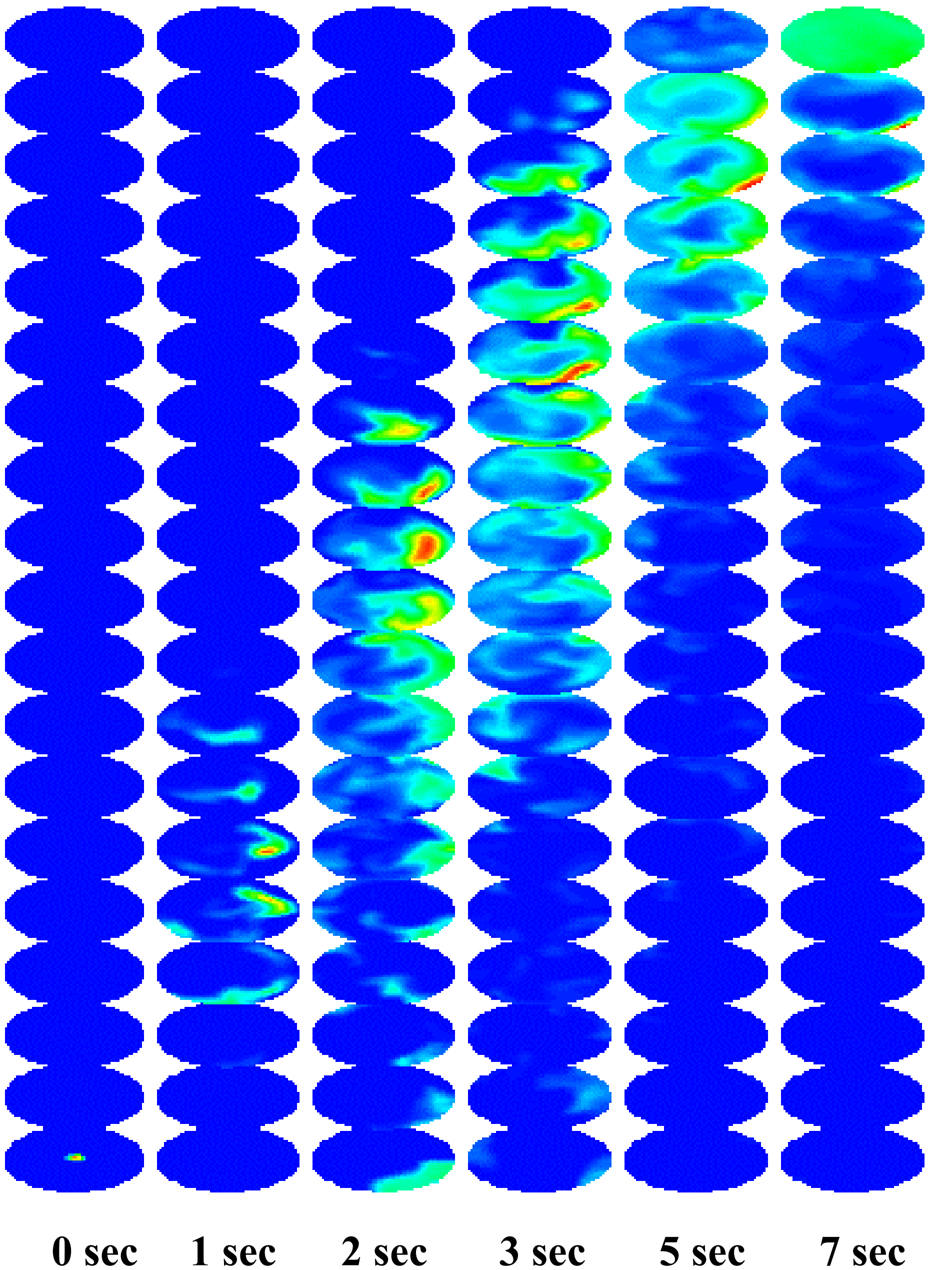

Figure 3.5 Time Evolution of the Gas Tracer Concentration Inside a 14-cm Diameter Column at U_g=2.4 cm/s. (The tracer is released at the center of the column, near the bottom, at time t=0.)

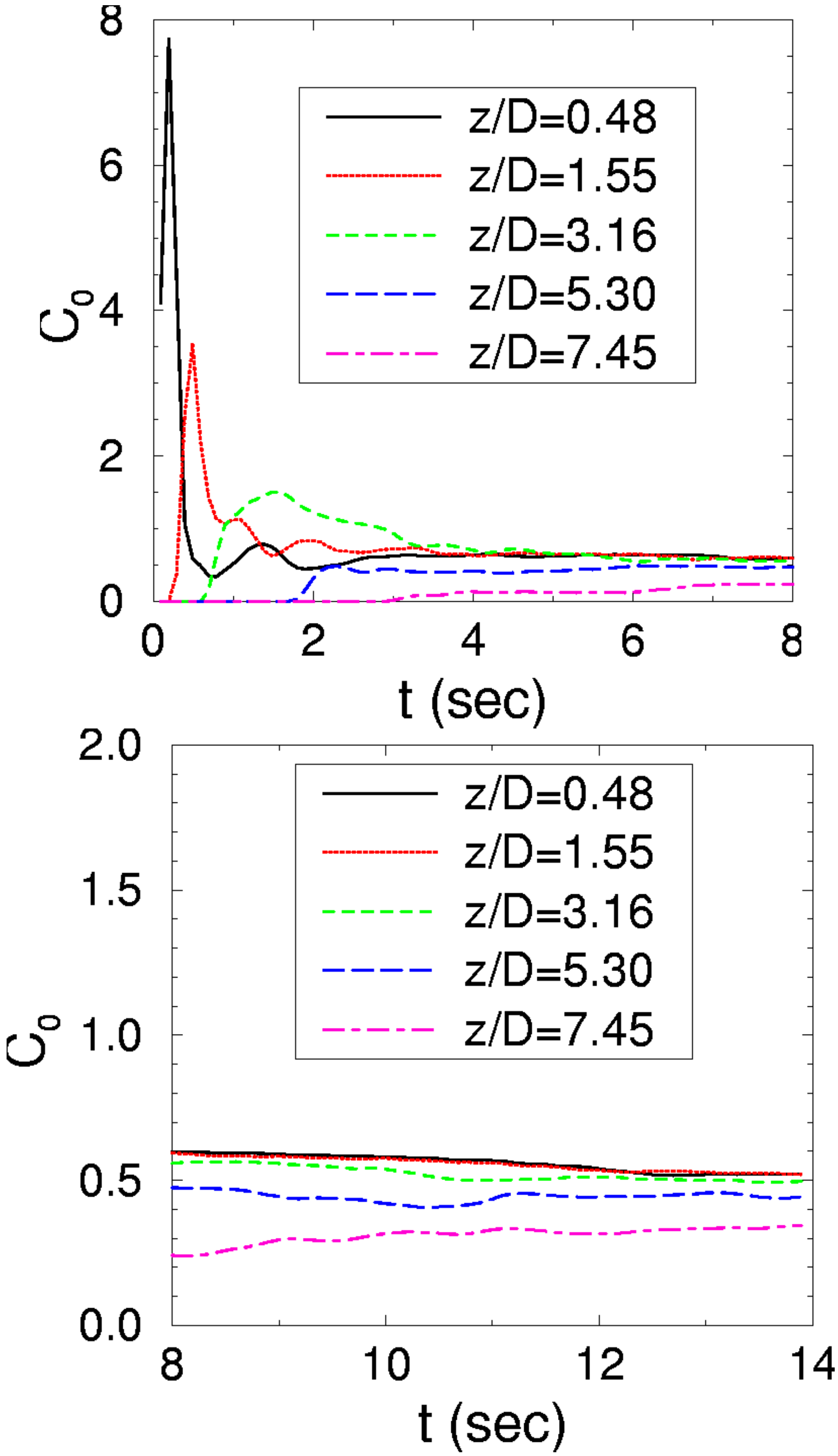

Figure 3.6 Numerical Detector Responses for Liquid Tracer Injection at r=0, z/D=0.2, in a 14-cm Column Operated at U_g=2.4 cm/s